Click Here for Full Article

Simulations of convectively-driven density currents in the Atlas region using a regional model: Impacts on dust emission and sensitivity to horizontal resolution and convection schemes

F. Reinfried,[1,2] I. Tegen,[1] B. Heinold,[1] O. Hellmuth,[1] K. Schepanski,[1,3] U. Cubasch,[4] H. Huebener,[4,5] and P. Knippertz[6]

[1]   During the SAMUM field campaign in southern Morocco in May and June 2006 density currents generated by evaporative cooling after convective precipitation were frequently observed at the Sahara side of the Atlas Mountain chain. The associated strong surface cold-air outflow during such events has been observed to lead to dust mobilization in the foothills. Here a regional model system is used to simulate a density current case on 3 June 2006 and the subsequent dust emission. The model studies are performed with different parameterization schemes for convection, and with different horizontal model grid resolutions to examine to which extent the model system can be used for reproducing dust emissions in this region. The effect of increasing the horizontal model grid resolution from 14 km to 2.8 km on the strength on the density currents and thus on dust emission is smaller than the differences due to different convection parameterization schemes in this case study. While the results in reproducing the observed density current at the Atlas Mountain varied with different convection parameterizations, the most realistic representation of the density current is obtained at 2.8 km grid resolution at which no parameterization of deep convection is needed.

1.   Introduction

[2]   Dust particles represent one of the major components of the global aerosol load. Mineral dust particles impact on the global and regional climate due to their radiative effects of scattering and absorption, their impact on cloud microphysics, and their effects on atmospheric chemistry. They cause great uncertainties in interpretation and projection of past and future climate changes [*Solomon et al.*, 2007]. A better understanding of dust processes (mobilization, transport and deposition) and improved prediction of the dust cycle is needed to enhance the understanding of dust as part of the climate system. As the atmospheric dust load is highly variable in time and space, the emission and the actual distribution of atmospheric mineral dust cannot be measured directly at large scales, but can only be estimated by model calculations [e.g., *Ginoux et al.*, 2001; *Tegen et al.*, 2002].

Such models usually predict dust distributions that are caused by large-scale frontal systems reasonably well. However, the comparably coarse model resolution makes the simulation of dust emission caused by small-scale processes difficult [*Cakmur et al.*, 2004]. The emission term, which is the most crucial part in dust simulations, depends mainly on the nature of the soil and the near-surface winds [*Laurent et al.*, 2008; *Tegen et al.*, 2002]. As the dust emission flux is proportional to the third power of the wind friction velocity, the accuracy of the surface winds in dust simulations is crucial [e.g., *Gillette and Passi*, 1988; *Shao et al.*, 1993]. Therefore, a realistic simulation of the meteorological conditions is a prerequisite to compute dust emissions correctly. Large scale atmospheric models that are used in climate and weather studies use a resolution that is spatially too coarse to resolve a number of meteorological phenomena explicitly, such as convective activity. To account for this problem subgrid-scale parameterization schemes have been developed. Particularly in orographically highly structured regions, the simulation of subgrid-scale processes such as convection and precipitation is very complex and frequently not correctly resolved [*Barthlott et al.*, 2006]. It is expected that higher resolved regional scale models are better suited to reproduce the characteristics of surface wind speeds, and in particular the maximum wind speeds, compared to global-scale models.

[3]   During the SAharan Mineral dUst experiMent (SAMUM, http://www.samum.tropos.de) in May and June

---

[1]Leibniz Institute for Tropospheric Research, Leipzig, Germany.
[2]Now at Ergo Institute of Environment, Emission/Imission, Dresden, Germany.
[3]Leibniz Institute of Marine Sciences, Kiel, Germany.
[4]Institute for Meteorology, Free University Berlin, Berlin, Germany.
[5]Now at Hessian Agency for Environment and Geology, Hessian Centre on Climate Change Affairs, Wiesbaden, Germany.
[6]Institute for Atmospheric Physics, Johannes Gutenberg University, Mainz, Germany.
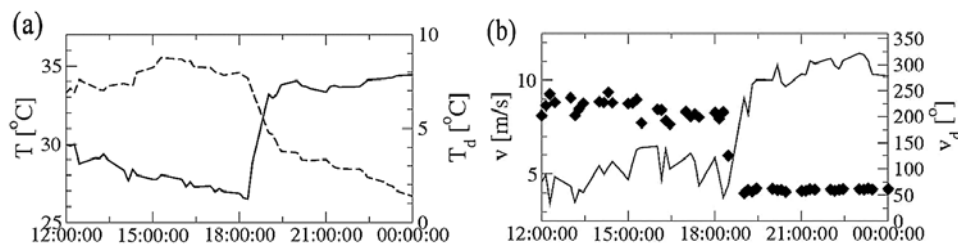
Figure 1. Characteristic changes of (a) 2-m air temperature T (dashed line) and 2-m dew point temperature T_d (solid line), and (b) 10-m wind velocity v (solid line) and wind direction v_d (diamonds) due to the passage of the density current on 3 June 2006 at the station El Myit, 30.36°N, 5.63°W.

2006 near Ouarzazate (Morocco) the occurrence of cold, moist airflows was frequently observed causing dust emission south of the Atlas Mountains. The mechanism responsible for such events is described in the work of *Knippertz et al.* [2007]. The authors attribute these observations to density currents generated by evaporative cooling after precipitation in high altitudes at the mountainside. Because of its increased density, the cooled air mass is considerably accelerated and propagates rapidly following the topographical gradient towards the Sahara. The vigorous cold-air outflow results in strong surface wind speeds at the leading edge of the density current so that atmospheric preconditions for dust mobilization are fulfilled. This process is enhanced by the eastward advection of hydrometeors to the Saharan side of the Atlas by strong westerly winds at upper levels [*Knippertz et al.*, 2009]. *Knippertz et al.* [2007] could clearly identify the passage of density currents in imagery of the Meteosat geostationary satellite and in measurements of the IMPETUS (An Integrated Approach to the Efficient Management of Scarce Water Resources in West Africa) station network. The authors note a strong increase in dew point temperature of around 8 K, a decrease in air temperature of around 4–7 K, a change in wind direction, and an acceleration of the wind velocity related to the density current passage [*Knippertz et al.*, 2007]. These characteristic changes are representatively shown in Figure 1 for a meteorological station south of the Atlas Mountains (El Myit, 30.36°N, 5.63°W) on 3 June 2006. As part of the regional climate they essentially contribute to the local dust mobilization, as they do in other mountainous regions of the Saharan desert.

[4] Here we investigate whether the regional model system LM-MUSCAT that was developed for simulating spatiotemporal characteristics of dust events that occurred during the SAMUM campaign [*Tegen et al.*, 2006; *Heinold et al.*, 2007, 2009; *Helmert et al.*, 2007] can reproduce the meteorological situation that initiates a density current, and test if the threshold friction velocity for dust mobilization is reached in the simulations. Being able to reproduce this phenomenon can help to improve the model configurations for other regions and in the following to study the dust effects. The study focuses on two aspects: The influence of the horizontal grid resolution, and the impact of different parameterizations of convection in the model.

2. Methodology

2.1. Model Description

[5] The meteorological model "Lokal Modell" (LM), now renamed COSMO, developed by the German weather service "Deutscher Wetterdienst" (DWD), is the key element of the operational numerical weather prediction since 1999 [*Steppeler et al.*, 2003]. This is a non-hydrostatic, high-resolution, limited-area model based on the primitive, unfiltered Eulerian equations of the thermo-hydrodynamic processes describing a compressible flow in a moist atmosphere. In the vertical, a generalized terrain following, time-independent coordinate is used. The distance of the vertical levels increases with height. An Arakawa-C-grid is used in the horizontal direction and a Lorenz-grid in the vertical. As a limited-area model the LM needs temporal and spatial boundary conditions from a large-scale model. The LM is initialized by the global model GME ("Global Model" of DWD) with a grid resolution of 60 km, or alternatively, by a LM run with lower grid resolution. At the starting time the LM receives the initial conditions (including soil moisture fields) from the GME or LM run, respectively, and adapts the temporal variable boundary data every 6 hours by interpolating to the LM grid. The LM-GME coupling and the zoom from a larger LM domain into a smaller one are realized by "one-way-nesting". In this study, the LM version 3.19 is used. A detailed model description is given by *Steppeler et al.* [2003]. LM has previously been used for the Atlas region in the Sahara, e.g. in a study investigating precipitation formation by *Huebener et al.* [2007].

[6] The LM has been used in this region in as part of the multi-scale model system LM-MUSCAT to compute Saharan dust emission and transport [*Heinold et al.*, 2007]. The Dust Emission Scheme (DES) coupled to LM-MUSCAT calculates dust emission fluxes applying the model developed by *Tegen et al.* [2002]. In this study an offline version of the dust emission scheme is used to compute dust emissions from LM surface winds simulated by the individual model realizations in this study. The mobilization of mineral dust occurs in active sources when the wind velocity exceeds a certain local threshold value. The surface friction velocity u_* as well as the threshold friction velocity u_{*t} for each particle size fraction is calculated in order to determine the time and size resolved dust fluxes [*Tegen et al.*, 2002]. Dust emission was suppressed in gridcells with a vegetation cover higher than 10% of the surface. For the purpose of dust emission computation the surface roughness was set to a constant value of 0.001 cm, and dust emission was calculated as independent from the soil moisture to obtain maximum possible dust emission fluxes. For simulations of Saharan dust events the vertical dust fluxes have been used as input for the online-coupled MUltiScale Chemistry Aerosol Transport Model (MUSCAT) [*Wolke et al.*, 2004] in previous studies

Table 1. Main Differences Between the *Tiedtke* [1989] and *Kain and Fritsch* [1993] Convection Schemes

	Tiedtke (TS-89)	Kain-Fritsch (KFS-93)
Source of convection activation	First model layer	60 hPa deep layer Including vertical velocity
Entrainment/detrainment rate	Fixed values	Variable detrainment rate
Minimum cloud depth for conversion rate	D_{min} = 1500 m over ocean D_{min} = 3000 m over land	$D_{min} = D_{min}$ (T_{LCL})
Closure assumption	Moisture convergence	Removal of CAPE

[*Tegen et al.*, 2006; *Heinold et al.*, 2007, 2009; *Helmert et al.*, 2007].

2.1.1. LM Moist Convection Parameterization

[7] Convective precipitation is essential for the generation of the density currents in South Morocco. In this study we used the convection schemes developed by *Tiedtke* [1989] and by *Kain and Fritsch* [1993]. Both are mass flux schemes calculating the transfer of mass from one vertical level to the next.

[8] A mass flux scheme requires a special averaging of the micro-turbulent equations for heat, moisture, and momentum to obtain prognostic equations for the grid-scale variables that describe the average conditions within a grid box. The horizontal area of averaging is assumed to be large enough to include a whole ensemble of clouds with all stages of formation, which is represented by their average values using a one-dimensional bulk cloud model after *Yanai et al.* [1973]. The aim of the convection schemes is to re-establish a stable local vertical structure in the model atmosphere. In this paper, only the main differences between the Tiedtke and the Kain-Fritsch schemes are presented. A detailed description of the Tiedtke convection scheme (hereafter TS-89) can be found in the work of *Tiedtke* [1989] as well as in the LM documentation of the DWD [*Doms and Schättler*, 2002]. The Kain-Fritsch scheme (hereafter KFS-93) is described in the work of *Kain and Fritsch* [1993] and in *Kain* [2004].

2.1.2. Main Differences Between the *Tiedtke* [1989] and *Kain and Fritsch* [1993] Convection Schemes

[9] Both schemes comprise a trigger function to activate convection. TS-89 triggers convection when the meteorological parameters of the first model layer (67 m for 14 km grid resolution) above the surface indicate unstable conditions. KFS-93 activates convection if the values of a 60 hPa deep layer indicate unstable conditions. Furthermore, it is suggested that convective development is favored by background vertical motion. Thus, a temperature perturbation is added to the air parcel temperature, which is linked to the magnitude of grid-resolved vertical motion [*Kain*, 2004].

[10] In TS-89, the conversion of cloud droplets into raindrops depends linearly on the updraft cloud water content and on an empirical height-dependent conversion function. The chosen formulation allows the generation of precipitation not until the minimum cloud depth D_{min} exceeds a certain value. In the LM, D_{min} is set equal to 1500 m over water and to 3000 m over land [*Doms et al.*, 2005]. The growth of raindrops due to collection is not considered explicitly. Processes of freezing and melting of ice particles are not taken into account [*Tiedtke*, 1989]. In KFS-93, the minimum cloud depth D_{min} is a function of the lifting condensation level temperature T_{LCL} (°C) [*Kain*, 2004]:

$$D_{min} = 2000 \text{ m} \qquad \text{for } T_{LCL} < 0°\text{C}$$

$$D_{min} = 2000 \text{ m} + 100 \cdot T_{LCL} \quad \text{for } 0°\text{C} \leq T_{LCL} \leq 20°\text{C}$$

$$D_{min} = 4000 \text{ m} \qquad \text{for } T_{LCL} > 20°\text{C}$$

Hence, the activation of deep convection is allowed for comparatively shallow clouds with active ice-phase processes [*Kain*, 2004]. When the cloud scheme computes updrafts that do not reach the minimum cloud depth for deep convection, shallow (non-precipitating) clouds are activated.

[11] The convection parameterization scheme causes a redistribution of mass in a convective cell by entrainment and detrainment, updrafts and downdrafts. In TS-89, the turbulent entrainment and detrainment are calculated by fixed rates that are chosen to allow the penetration of clouds to high levels for tropical deep convective clouds. For shallow convection, typical for larger trade wind cumuli, the values are chosen to inhibit small clouds with large entrainment/detrainment rates. In KFS-93, the maximum possible entrainment rate, at which environmental air mixes into the turbulent region of an updraft over a pressure interval, is controlled by the specified cloud updraft radius that depends on large-scale forcing [*Kain*, 2004]. Additionally, a minimum entrainment rate is implemented in the KFS-93 to avoid hypersensitive activation of deep convection [*Kain*, 2004].

[12] The two parameterization schemes use different closure assumptions. In TS-89, a moisture balance for the low-level sub-cloud layer is imposed such that the cloud mass flux is linked to the low-level, large-scale moisture convergence [*Kuo*, 1965]. According to *Tiedtke* [1989], this closure assumption is well justified over tropical oceans. In that region the moisture content of the boundary layer typically changes little with time. However, there is no verification for other regions [*Doms et al.*, 2005]. The KFS-93 uses a CAPE (convective available potential energy) closure. To rearrange stability in the grid cell, the CAPE in the environment has to be eliminated by convection. Therefore, the mass fluxes are increased incrementally via convective updrafts and downdrafts until at least 90 % of CAPE is removed. The CAPE closure depends entirely on the thermodynamic characteristics of the atmosphere. Organized convection, its longevity, and other properties affected by wind profiles are not part of the closure [*Kain*, 2004]. The main differences between the two schemes are summarized in Table 1.

2.2. Model Setup

[13] With respect to the treatment of moist convection in the model system, three different model setups were used, including the Tiedtke convection parameterization scheme (TS-89), the Kain-Fritsch convection parameterization scheme (KFS-93); and no explicit convection parameterization (NC). For the investigation of the impact of the model grid resolution we conducted model runs with horizontal grid resolutions of 2.8 km, 7 km and 14 km. The simulations of higher grid resolution are nested into the next lower resolution by "one-way-nesting" with the model runs using the TS-89 at the coarser resolution. The performance of model runs with 14 and 7 km grid resolution without
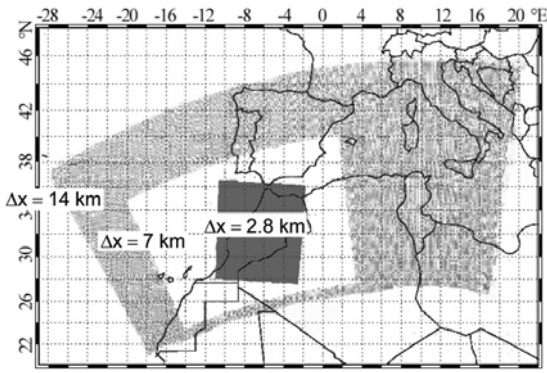
Figure 2. Model domain of the model runs with 14 km grid resolution, 7 km grid resolution, and 2.8 km grid resolution.

convection parameterization is not a standard method and is only considered as sensitivity study. Details of the model setup are given in Table 2. The model domains are shown in Figure 2.

2.3. Meteorological Data

[14] The model output is compared with the measurements of the IMPETUS stations that are situated along the Drâa valley following a north-south transect from the peaks of the High Atlas (up to 3850 m) down to the margin of the Sahara (445 m) (Figure 3). From those stations measurements of 2-m air temperature $T(°C)$, 2-m dew point temperature $T_d(°C)$, wind velocity v (m s^{-1}) in 3 m height, and wind direction v_d (degree) are available every 15 min for the studied period. As a representative measurement site for the verification of the model results, the station El Myit (EMY hereafter; 30.36°N, 5.63°W, 792 m a.s.l.), located in the foreland of the Atlas Mountains (Figure 3), is used. Apart from the IMPETUS data, hardly any observational station data are available in this region. Some data are available from satellite remote sensing. The density current event that occurred on 3 June and is simulated for the analyses presented in this paper was observed in satellite data and is described in detail in *Knippertz et al.* [2007]. In this paper, the modeled precipitation rates are compared with precipitation information derived by the Tropical Rainfall Measuring Mission (TRMM 3B42 V6, http://disc2.nascom.nasa.gov/Giovanni/tovas/). These data are derived from the joint Japan-U.S. cooperative Earth Probe satellite comprising a rain radar, a multi-channel passive microwave sensor, and a sensor of a live-channel Visible/Infrared radiometer [*Simpson et al.*, 1996].

3. Results

3.1. Meteorological Situation on 3 June 2006

[15] The period from 2–5 June 2006 is characterized by an upper-level trough, located over the central Mediterranean, moving slowly eastward, and an almost stationary upper-level trough over the Azores. A ridge is located in between close to the Iberian Peninsula. Its local maximum is situated north of the investigation area. On the southern side of this ridge, a pressure gradient induces an eastward to north-eastward flow in the free troposphere over Morocco. This north-eastward flow with strong vertical wind shear provokes the formation of deep convective clouds over the elevated terrain of the Atlas Mountains that are advected towards the Saharan side of the Atlas chain [*Knippertz et al.*, 2007]. Due to a high pressure system over Algeria, westward to south-westward winds are induced to the south of the Atlas Mountains transporting dry and hot air masses into that region.

[16] On each of these days cellular convection developed over the Atlas around noontime. Precipitation is recorded in the High Atlas by the IMPETUS stations at noon and during the afternoons leading to an outflow of cold air from the rainfall area towards the Sahara. This leads to the formation of density currents on each day between 2 June and 5 June [*Knippertz et al.*, 2007]. The investigation focuses on June 3 being representative to study the ability of the model to reproduce a realistic density current.

[17] On 3 June precipitation starts around 12 UTC in the High Atlas. The convective clouds are advected towards the Sahara and farther south-eastward during the afternoon with the mean upper-level flow (500 hPa). The IMPETUS stations located south of the High Atlas indicate the passage of the density current by the characteristic changes, which is representatively shown for station EMY on 3 June 2006 around 18 UTC: The decrease in T, the increase in T_d (Figure 1a), the increase in v, and the change in wind direction v_d (Figure 1b). The leading edge of the current extends over several 100 km. Until 02 UTC on 4 June the cold air moving towards south-western Algeria can still be identified in Meteosat satellite images [*Knippertz et al.*, 2007] and Multi-angle Imaging SpectroRadiometer (MISR) observations [*Kahn et al.*, 2009].

Table 2. Model Setup for the Individual Runs With Different Model Grid Resolutions and With Application of Different Convection Parameterization Schemes (Tiedtke Scheme (TS-89), Kain-Fritsch Scheme (KFS-93), and Without Explicit Convection Parameterization (NC))

| LM 3.19	14 km			7 km			2.8 km
Horizontal grid spacing Δx	0.125° (= 14 km)			0.0625° (= 7 km)			0.025° (= 2.8 km)
Number of grid points in model domain	300 × 150 × 40			300 × 200 × 40			300 × 340 × 50
Depth of lowest layer	67 m			67 m			25 m
Number of vertical layers	40			40			50
Time step	45 s			30 s			15 s
Outer grid	GME			LM 14 km			LM 7 km
Boundary conditions	Each 6 hours			Hourly			Hourly
Grid-scale microphysics parameterization	"graupel" scheme [*Doms and Schättler*, 2002; *Reinhardt*, 2005]						
Subgrid-scale convection parameterization	TS-89	KFS-93	NC	TS-89	KFS-93	NC	NC
Initialisation and run time	01.06.2006, 12:00 UTC + 96h			02.06.2006, 00:00 UTC + 84h			02.06.2006, 06:00 UTC + 78h
Denotation	T-14	KF-14	NC-14	T-7	KF-7	NC-7	NC-2.8
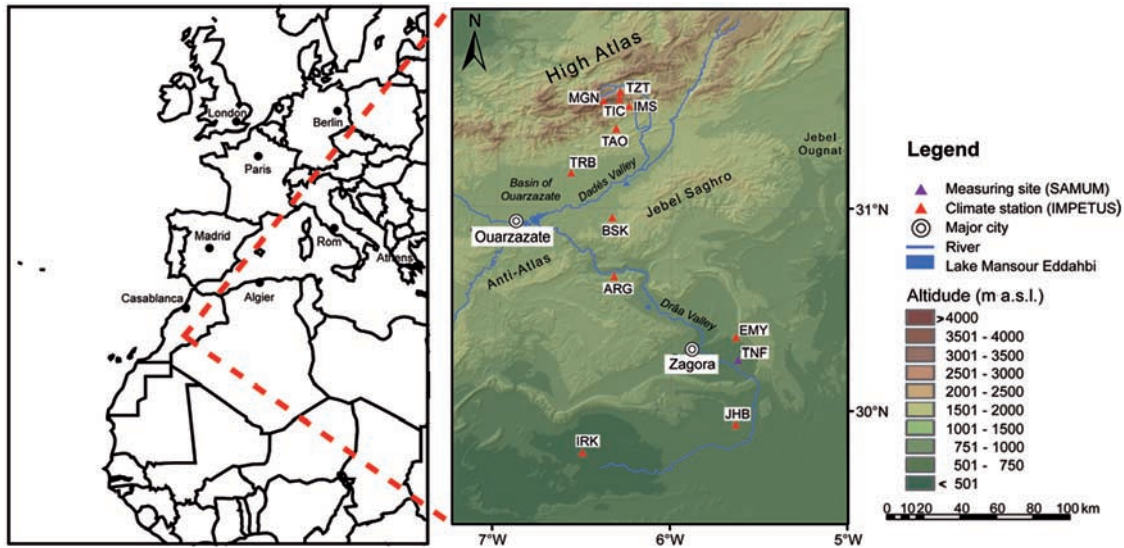
Figure 3. Investigation area and location of IMPETUS stations, redrawn from *Knippertz et al.* [2007].

3.2. Sensitivity of Simulations to Different Convection Parameterization Schemes

[18] Simulating the meteorological phenomenon of the density current in South Morocco, we performed model runs using the TS-89 and KFS-93 convection parameterizations, respectively. We also performed model runs without convection parameterization. The three simulations (T-14, KF-14, NC-14, and Table 2) are initialized in the same way. We focus on simulating the event with 14 km model grid resolution because at this resolution the model LM-MUSCAT has been used previously to characterize individual dust outbreaks [*Heinold et al.*, 2007; *Helmert et al.*, 2007]. While more realistic results are expected at higher model resolution, an objective of this study is to test to which extent the model reproduces events leading to dust mobilization for a model setup that is useful for investigations of large-scale Saharan dust events. Such investigations require large model domains and very high grid resolutions are not feasible. A qualitative summary of the model's ability to reproduce the observed meteorological features are given in Table 3.

[19] The large-scale meteorological situation is comparably reproduced by T-14, KF-14, and NC-14. However, the model results differ considerably in simulating precipitation and, consequently, in reproducing the observed density current. The onset of precipitation over the High Atlas around 12 UTC, recorded by the IMPETUS mountain stations (not shown), was correctly predicted only by KF-14.
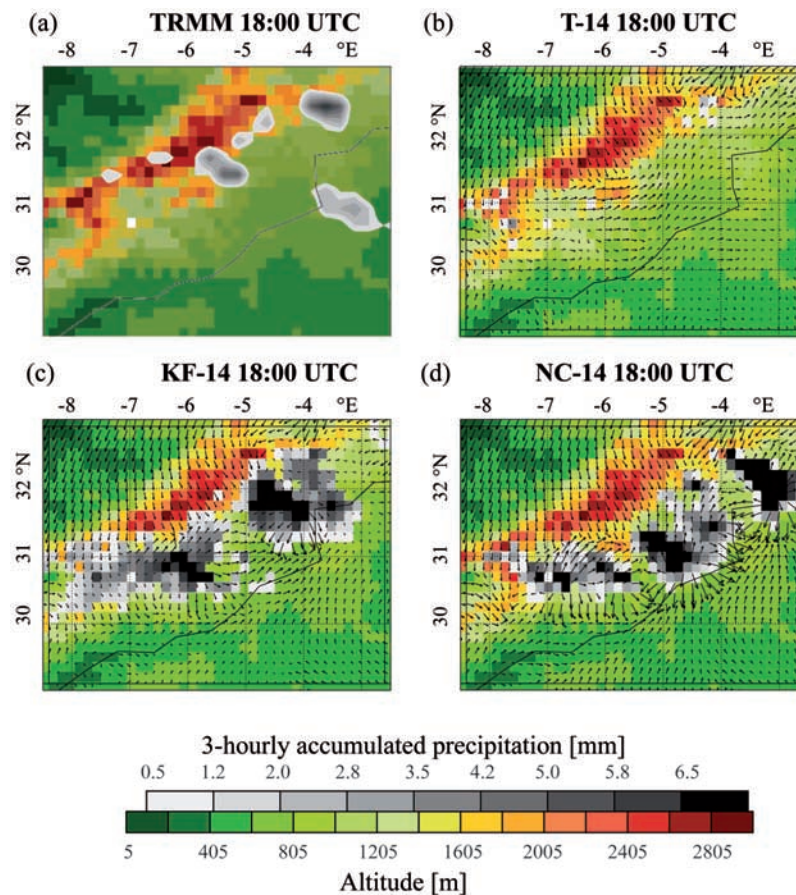
Figure 4a shows the accumulated precipitation between 15 and 18 UTC as obtained from TRMM data. In model run T-14 (Figure 4b) none of the three maxima depicted by the TRMM data are reproduced. Only some grid boxes in the High Atlas show precipitation, but the extent and rain rates are highly underestimated. In the runs NC-14 and T-14 precipitation forms a little later (around 13 UTC) than observed (not shown). In the afternoon between 15 and 18 UTC, the amount of precipitation is overestimated in KF-14 (Figure 4c) and even more so in NC-14 (Figure 4d), which yields an approximately 40% higher accumulated rainfall compared to TRMM data (Figure 4a). Some disagreement between model results and the TRMM data may be explained by a dry bias in the satellite product. E.g. *Dinku et al.* [2008] find a relative bias of 0.84 between the TRMM product and station observations for complex terrain in Ethiopia. In both simulations, the spatial extent of the 3-hourly accumulated rainfall fields is too large and shifted to south-easterly directions compared to TRMM data. For example, both KF-14 and NC-14 predict precipitation over the Drâa-Valley (31.3–29.8°N, 5.6–6.5°W), although rainfall was not observed at this location during this time.

[20] Furthermore, we evaluated the simulation of divergent outflows from convective systems. The model runs NC-14 and KF-14 reveal divergent outflow areas at the southern side of the Atlas Mountains, which can be seen in the simulated 10-m wind fields (Figures 4c and 4d). They are clearly connected to the precipitation fields indicating

Table 3. Summary of the Main Qualitative Model Results Regarding the Simulation of the Density Current on 3 June[a]

		NC-14	KF-14	T-14	NC-7	KF-7	T-7	NC-2.8
Characteristics of the density current Passage	Decrease of T	+	=	−−	=	=	+	+
	Increase of T_d	+	+	−−	+	++	++	=
	Increase of v	=	−	−−	=	=	−	=
Wind velocity maxima		=	−	−−	=	=	−−	=
Onset of precipitation		−	=	−	−	=	=	=
Amount of precipitation		++	+	−−	++	+	−	++
Extent of precipitation fields		++	++	−−	++	++	−	++

[a]=, in agreement with measurements; +, overestimated; ++, strongly overestimated; −, underestimated; −−, strongly underestimated compared to measurements.

Figure 4. (a) 3-hourly accumulated precipitation derived from TRMM data on 3 June 2006 15–18 UTC over the investigation area (http://disc2.nascom.nasa.gov/Giovanni/tovas/); 10-m wind field (arrows) and 3-hourly accumulated precipitation between 15 and 18 UTC (white and grey pixels) over the model orography (colored) of T-14 (b), KF-14 (c), NC-14 (d) on 3 June 18 UTC.

cooled descending air masses. In both runs, such outflows were simulated over the Drâa-Valley. The high wind velocities up to 15 m s^{-1}, simulated by NC-14, are slightly higher than measurements for the precipitation event. At the station EMY the maximum wind speeds that were observed for this episode were at 12 m s^{-1} (Figure 5). In contrast to this results, the 10-m flow pattern of T-14 (Figure 4b) shows an almost homogeneous wind field, i.e., without any divergent outflow areas. This effect is a direct consequence of the suppressed rain formation in the T-14 simulation at this time.

[21] The time series of measurements and model results at EMY are shown in Figure 5. During the time period between 1 June 2006 12 UTC and 4 June, 6 UTC density currents are evident in the measurements on 2 June, 19 UTC and 3 June, 18 UTC by increasing dew point temperatures T_d and surface wind speeds. The increase of T_d caused by the density currents is reproduced by KF-14 and NC 14 on both days, but is underestimated and occurs too early on 2 June. In T-14 the meteorological parameters do not indicate a passage of density currents during this time period. Generally, all simulations show a too pronounced diurnal cycle of T and a moist bias. The daily temperature maximum occurs too early in the model compared to the station observations, while the nocturnal minimum is reproduced at the correct time.

[22] Regarding the reproduction of the density current passage, the time series highlights the differences between the different model realizations. In comparison to the observations on 3 June (black line), the simulation NC-14 (green line) is able to reproduce the characteristic changes due to the passage of the density current with respect to both their most pronounced features and the time of their onset, although it is not usual practice to use a model setup at 14 km without convection parameterization. Regarding the temperature, the results of KF-14 (red line) are closest to the measurements and lie in between the results of NC-14 and T-14 (blue line) (Figure 5, top). For the same day, KF-14 and NC-14 reproduce a sharp increase in T_d (Figure 5, middle) associated to the density current, but overestimate the increase by approximately 5 K. T-14 does not reproduce that sharp increase. Good results are obtained for NC-14 in reproducing the wind velocity (Figure 5, bottom) indicating the wind speed maxima on 3 June. Also, run KF-14 simulates the increase in the wind velocity due to the density current passage. However, the maxima of surface wind speed v, required to initiate dust emission, are underestimated. The scatter plot of model results and observations (Figure 5, lower right panel) illustrates in particular the underestimate of maximum v of the model run T-14.

[23] In summary, the capability of the regional model to reproduce the observed case of a density current formation in South Morocco highly depends on the choice of the convection scheme. While the model simulation using
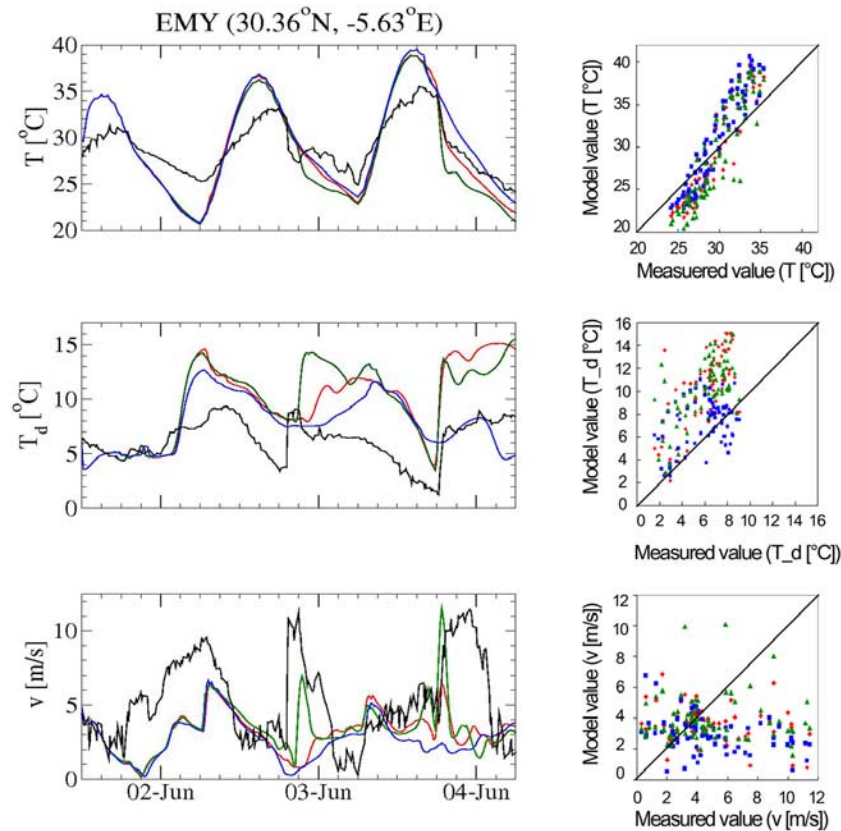
Figure 5. (left) Time series of *T, T_d,v* for NC-14 (green), KF-14 (red), T-14 (blue), and measurements (black) at EMY. (right) Scatter plots of model values versus measured values of the corresponding parameter (colors as above) from 1 June 2006 12 UTC to 4 June 2006 06 UTC.

KF-93 and the one without convection parameterization are able to reproduce the passage of the density current on 3 June 2006, the simulation using TS-89 fails to reproduce precipitation and thus the formation of a density current in this particular case.

[24] The considerable difference in the cloud cover, especially that of high clouds, between T-14 and the two other simulations gives a strong hint at possible reasons for failure in the prediction of the density current by TS-89. The model runs KF-14 and NC-14 produce almost identical cloud patterns in this period. However, with TS-89 the cloud pattern changes considerably. Particularly, the simulated coverage with mid-level (not shown) and high clouds (Figure 6) in T-14 is larger and more persistent compared to KF-14. Between 15 and 18 UTC, the cloud cover remains high and even increases with time in T-14, while in KF-14 the cloud cover decreases.

[25] As mentioned above, TS-89 uses fixed values for the entrainment/detrainment rates, which were empirically adjusted to the hydrothermodynamic conditions in the Inter Tropical Convergence Zone. The corresponding parameters for tropical thunderstorm clouds allow deep convection to penetrate to high levels, while the parameter for shallow convection (typical for larger trade wind cumuli) inhibit the formation of small clouds with large entrainment/detrainment rates above their cloud bases [*Tiedtke*, 1989]. Thus, apparently this scheme has a tendency to promote

effective moisture transport to the upper model levels. While under tropical conditions such performance is wanted, in arid regions it is very likely to cause failure predictions of moist convection and associated phenomena, such as density currents. Therefore, any application of an empirically adjusted model outside of the conditions of its validity deserves a careful revision of the empirical parameters and a re-evaluation of the model. As a consequence of the hypersensitive moisture transport of TS-89 in arid regions, the linear relationship that is assumed in TS-89 between convective cloud water and convective rain water might not be effective enough to produce rainfall in the model. Thus, the moisture transported upward, could be effectively transformed into cloud ice, which is considered in the grid-scale microphysical parameterization. In this way, a very fast vertical transport of moisture promotes the ice formation at high levels at the expense of rain formation at lower levels. One has to consider that the subsequent generation of precipitation from high ice clouds is less efficient than from the liquid phase. Consequently, the rain misprediction in T-14 is likely a result of the response of the grid-scale microphysical scheme to the moisture transport originating from the subgrid-scale convection scheme.

[26] Figure 7 illustrates the simulated cloud ice content accumulated over all levels of the grid column of T-14 (top), KF-14 (middle), and NC-14 (bottom) on 3 June, 15 UTC (left) and 18 UTC (right). While the cloud ice content
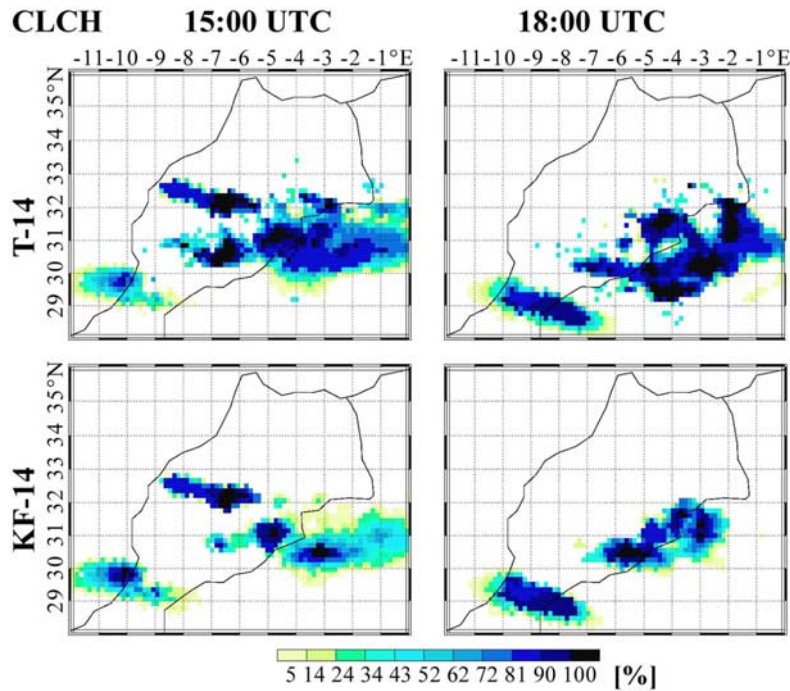
Figure 6.   Modeled cover of high clouds of T-14 and KF-14 on 3 June 2006 15 UTC and 18 UTC.
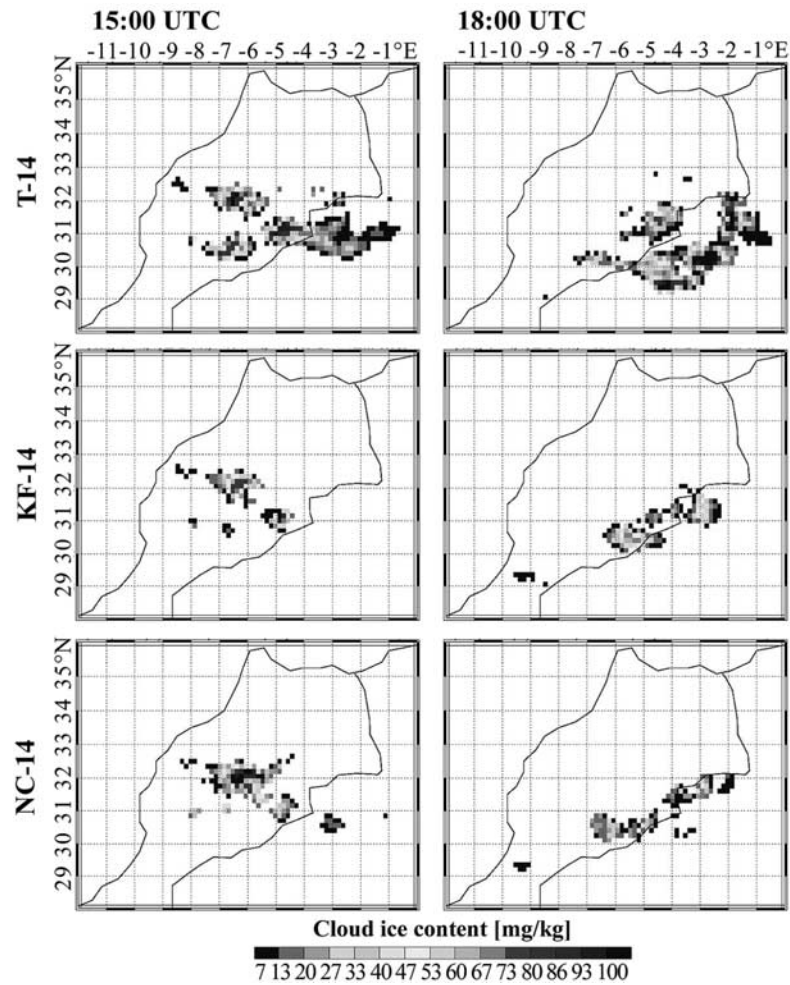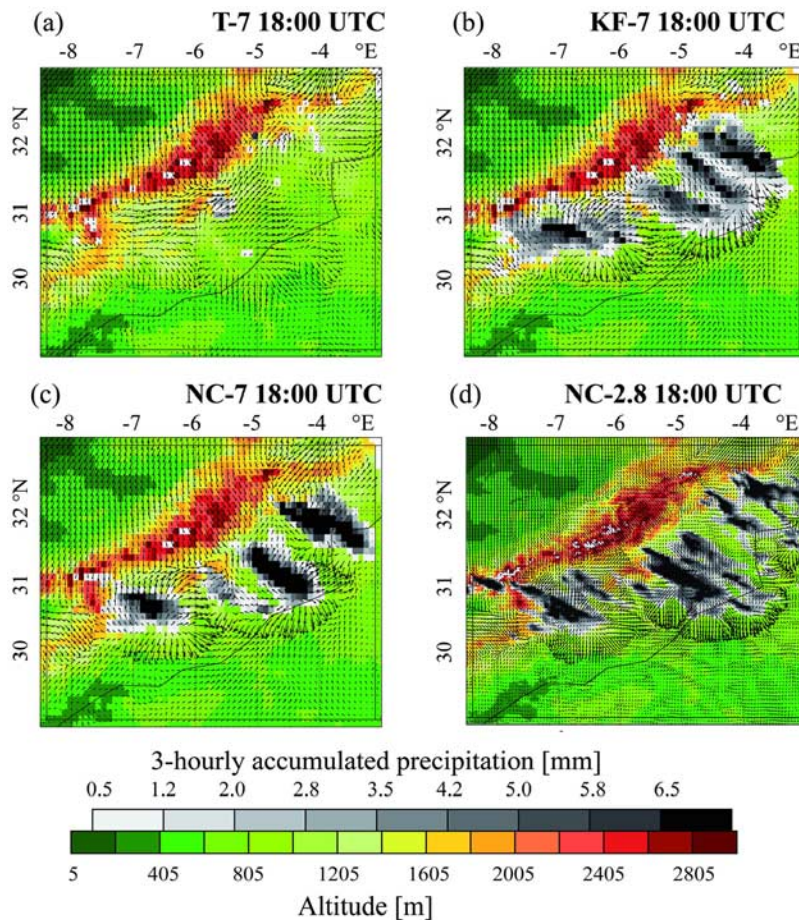

Figure 7.   Cloud ice content of T-14, KF-14, NC-14 for 3 June 2006 15 UTC and 18 UTC.

Figure 8. As Figure 4, but for T-7 (a), KF-7 (b), NC-7 (c), and NC-2.8 (d).

produced in the run KF-14 and NC-14 is similar, considerably more cloud ice is produced in T-14 at 15 UTC (Figure 7). At 18 UTC the cloud ice content is reduced in NC-14 and in KF-14 compared to 15 UTC. By contrast, T-14 produces a higher content of cloud ice compared to NC-14, KF-14 and compared to 15 UTC.

[27] Humidity is removed from the atmosphere by KFS-93 and by the grid-scale parameterization through precipitation. In contrast, moisture remains in the atmosphere in the form of cloud ice and no precipitation is generated by the TS-89 scheme. As a consequence, the pool of sufficiently cold air could not form and the density current is not captured. Processes like melting and freezing are not considered in the TS-89. This is an a-priori inconsistency with respect to the grid-scale ''graupel''-scheme [*Doms and Schättler*, 2002; *Reinhardt*, 2005], which includes snow, graupel and cloud ice (see also Table 1).

3.3. Sensitivity of Simulations to Different Horizontal Model Grid Resolutions

[28] To determine the sensitivity of the simulation results against the horizontal grid resolution, in addition to the 14 km resolution model runs (NC-14, KF-14, T-14) further runs on 7 km (NC-7, KF-7, T-7) and 2.8 km (NC-2.8) grids were performed (Table 2). For increased grid resolution to

the scale of deep convective clouds on the order of a few kilometers, improved model results are expected [*Ament et al.*, 2004]. The model characteristics with regard to reproducing the density current on 3 June 2006 are summarized in Table 3.

[29] The model results improve only slightly for T-7 (Figure 8a) compared to the coarser resolution of T-14 (Figure 4b). Although rainfall is still underestimated in T-7, the precipitation field over the Jebel Saghro (around 31.2°N, 5.7°W) is simulated, which is in agreement with TRMM data (Figure 4a). The associated divergent outflow of cooler air at the surface appears in the horizontal 10-m wind field. The model results do not considerable change in NC-7 and KF-7 (Figures 8b, 8c) compared to the reference run with 14 km grid resolution. The precipitation patterns change insignificantly compared to NC-14 and KF-14 (Figures 4c, 4d). Precipitation rates between 15 and 18 UTC in NC-7 and KF-7 remain overestimated, and the corresponding rainfall pattern is farther extended than found from observation. Connected to the precipitation events, the divergent outflow with high wind speeds at the leading edge is simulated by both NC-7 and KF-7.

[30] The temporal characteristics of T, T_d, and v, associated to the passage of the density current, are more pronounced and are reproduced at the correct time by NC-7 and KF-7
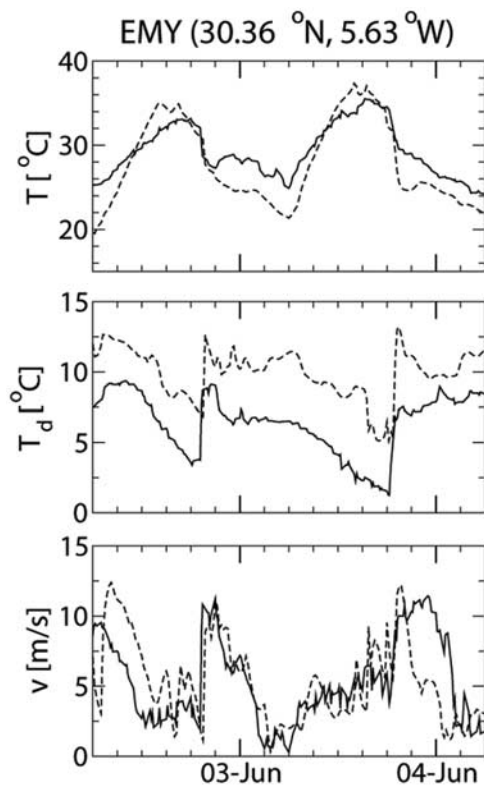
Figure 9. Time series of T, T_d, v for NC-2.8 (dashed line) and measurements (solid line) from 2 June 2006 06 UTC to 4 June 2006 06 UTC at EMY.

compared to observations on 3 June. The observed wind speed maximum at EMY and all other IMPETUS stations is better predicted in KF-7 than in KF-14, which is related to the slightly shifted precipitation field over the Drâa valley. In T-7, the density current passage is simulated only weak and too early. Thus, the expected wind maximum is highly underestimated and occurs too early compared to the observations. At the time of the passage of the density current the wind speed has reached a minimum.

[31] The model run with 2.8 km horizontal grid resolution without explicit parameterization of moist convection (NC-2.8; Figure 8d) overestimates the rainfall rates compared to TRMM data, as in cases NC-14 and NC-7. The results indicate huge outflow areas with strong horizontal convergences at the leading edges of the density currents with surface wind speeds of up to 18 m s^{-1}. However, comparing the time series and measurements best results are obtained with NC-2.8 (Figure 9): The characteristics of the density current and its passage are reproduced at the correct time, and the deviations in the time series from measurements are smallest compared to the other simulations. Especially, the simulated wind velocity, being evident for dust mobilization, is in very good agreement with measurements and high wind speeds are reproduced.

[32] In summary, the model runs using TS-89 highly underestimate precipitation by around 70–100% and, in consequence, do not simulate the observed density current. The model run with 7 km grid resolution (T-7) predicts the density current on 3 June to some extent, but too weak and

too early. Using KFS-93 or no convection parameterization scheme, the model results do not improve considerably when increasing the model grid spacing. The meteorological situation, precipitation pattern, and wind field change only slightly. Best results are obtained with 2.8 km grid resolution without explicit parameterization of moist convection (NC-2.8) in reproducing the characteristic changes associated to the density current.

[33] The large differences between the model runs with explicitly resolved convection, the model runs using KF-93, and TS-89, respectively, illustrate the influence of the convection parameterization for reproducing the process of density current generation in the Atlas Mountains. The differences in precipitation formation are influenced more strongly by the use of the convection parameterization than by the model grid resolution itself. Although precipitation is overestimated, the density current is simulated closest to the observations if no convection parameterization or KFS-93 is used due to the stronger formation of precipitation compared to TS-89.

3.4. Dust Emission

[34] Due to the strong surface winds at the leading edge of the density current, mineral dust can be mobilized. Local dust emission was recorded on June 3 after 17 UTC at Tinfou (TNF; 30.25°N, 5.62°W) by a Differential Mobility Particle Sizer (DMPS) and an Aerodynamic Particle Sizer (APS) combination that were operating during the SAMUM field campaign [*Kandler et al.*, 2009; *Schladitz et al.*, 2009]. On 3 June the daily averaged measured concentration of total suspended particles at TNF is about 600 μg m^{-3} [*Kandler et al.*, 2009]. The horizontal visibility remained below 10 km on this day [*Knippertz et al.*, 2009].

[35] For calculating dust emission on 3 June in the study area, the model results of T-14 and NC-2.8 are presented. The run T-14 is chosen because the TS-89 scheme has been used for the SAMUM computations [*Heinold et al.*, 2007]. For comparison, dust emissions computed within run NC-2.8 are shown, as the model at this resolution without convection parameterization reproduces the meteorological situation of the density current most realistically. Figure 10 shows the simulated dust emission (g m^{-2} h^{-1}) computed at 18 UTC. In the absence of high wind speeds, no dust emission is calculated in the model. As the simulation T-14 does not reproduce the density current and thus does not produce high surface wind speeds no dust emission is generated (Figure 10a). Some dust mobilization was computed by T-14 north of TNF, but in most grid cells in the area the modeled surface wind speeds remained below the threshold for dust emission. The emitted dust is transported in northeastward direction in this model run. However, in NC-2.8 more than 10 g m^{-2} h^{-1} of dust is emitted over a considerable area close to the Moroccan-Algerian border at 18 UTC hours (Figure 10b). Dust mobilization mainly occurs at the leading edge of the density current discussed above. Dust emission is simulated in the direct vicinity of TNF, which is in agreement with the observed enhanced dust concentration on that day. In an area of 1° × 1° around the location of TNF (lower left corner of area: 29.75°N, 6.12°W; upper right corner of area: 30.75°N, 5.12°W average dust emissions at 18 UTC are 0.9 g m^{-1} h^{-1}. Compared to this value, average
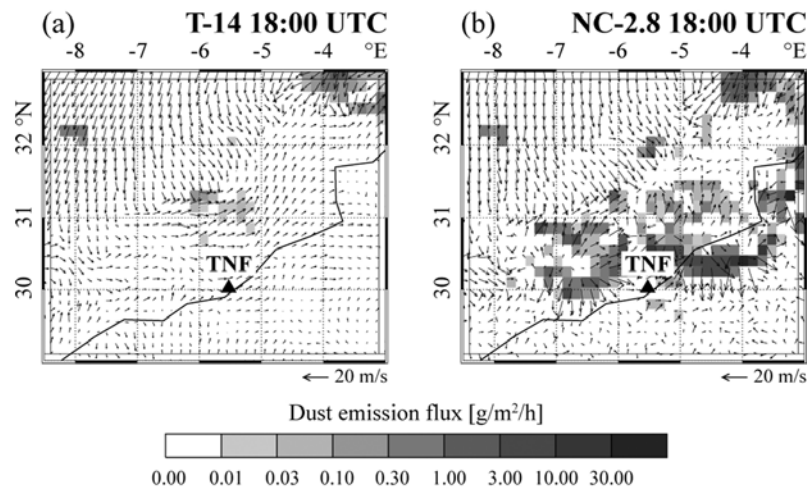
Figure 10. Wind field of the first model level (arrows) and the calculated dust emission (g m^{-2} h^{-1}) (grayscale) on 3 June 2006 18 UTC for T-14 (a) and NC-2.8 (b).

dust emissions in T-14 are approximately 3 orders of magnitude smaller at 0.0005 g m^{-1} h^{-1}. Observations during the period from 2–5 June point out that dust emission within the Drâa Valley originates in wadis or smaller topographic depression, and are thus very localized [*Knippertz et al.*, 2007]. The model resolution is too coarse to resolve such features, so that remaining misrepresentations in local dust emission may be due to oversimplification in the soil data. In general, the verification of the dust emission simulations is difficult as measurements are only available within the Drâa valley.

4. Discussion

[36] Simulations of regional meteorology and dust emission in the Atlas region during the period of the SAMUM experiment were carried out with the model system LM-MUSCAT-DES for the beginning of June 2006. The meteorological phenomenon of a density current generated by evaporative cooling of precipitation that lead to dust mobilization observed during SAMUM [*Knippertz et al.*, 2007] was simulated at different grid resolutions with the Tiedtke convection parameterization scheme (T-14, T-7), with the Kain-Fritsch scheme (KF-14, KF-7), and without convection parameterization (NC-14, NC-7, NC-2.8) (the numbers indicating the horizontal grid resolution in km).

[37] The model results substantially differ in terms of the representation of the density current on 3 June 2006, mainly related to the skill in reproducing convective precipitation. The model simulations with TS-89 underestimate the amount of precipitation irrespective of the horizontal grid resolution, and the density current is not reproduced. In this case, moisture is transported to higher model levels too efficiently, which enhances the formation of cloud ice. The model with KFS-93 correctly reproduces the temporal development of precipitation in time, but overestimates the amount and the extent of the precipitation region compared to satellite information. Nevertheless, the model run with KFS-93 simulates the main characteristics of the density current for this specific case. Without convection parameterization

the density current is even more pronounced and high wind speeds are simulated. However, amount and extent of the precipitation fields are highly overestimated. Only at the highest resolution the model should be run without convection parameterization.

[38] The underestimated rainfall rates with TS-89 in this case study may be caused by the fact that the constant values in the scheme are adjusted for the mid-latitudes (e.g., evaporation rate, conversion rate, turbulent length scale) and for the tropics (e.g., entrainment/detrainment rate). The results suggest that application of TS-89 to outer-European regions needs an adaptation of the parameters in the convection scheme to the specific region, especially if convection plays an essential role. As KFS-93 uses more variable functions of the parameters, this convection scheme can be applied to this region more easily. For this case we found that this scheme provided better results in the simulations of the development of precipitation and the density current at the Atlas Mountains. Here, the impact of changing the model grid resolution is less pronounced compared to the influence of the convection schemes.

[39] Dust emission is a threshold phenomenon. Thus, small failures in the calculated surface wind speeds or friction velocities can cause considerable errors in dust emission calculations. This study illustrates in particular that shortcomings in the convection parameterization and in consequence too low simulated surface wind speeds adversely affect the model ability to produce realistic dust emissions. Besides the convection parameterization scheme, the energy transfer at the surface and the turbulent fluxes of momentum, moisture, and temperature in the planetary boundary layer are critical parameters influencing both the generation of the density current as well as dust mobilization and transport. Recent modeling experiments by one of the authors, *Knippertz et al.* [2007], have revealed a significant sensitivity of convectively-driven density currents to the turbulence length scale in the boundary layer and to the chosen raindrop size distribution. The meteorological situation of the density current formation at the Atlas Mountains and the dust emission related to this event is best reproduced by the

model with highest grid resolution and without convection parameterization. While for investigations of Saharan dust emission and transport computations at this high resolution are still computationally too expensive to be used as a standard model setup, such results can be used as benchmark for model simulations at coarser resolution.

[40] Up to now not all microphysical processes within clouds are completely understood. The development of convection parameterization is an ongoing process. Both TS-89 and KFS-93 are continuously improved through new computational possibilities and a better understanding of the grid scale and sub-grid scale microphysical processes.

[41] The DWD now uses a modified CAPE closure in TS-89, parameterizing only shallow convection in a 2.8 km grid resolution operational working model. The performance of KFS-93 will be tested for other SAMUM computations, and for other regions where moist convection plays an important role for dust generation. A useful study will be to test how the fixed parameters in TS-89 need to be adjusted such that the model would reproduce the rainfall and density current of this case study, using the simulation NC-2.8 as benchmark.

[42] In earlier work the regional model used in this study, e.g., *Heinold et al.* [2007], has performed satisfactorily, in particular for dust mobilization events that were due to synoptic-scale weather systems. However, especially in the Sahara region, moist convection is of crucial importance for the generation of dust events while the parameterization of moist convection has a strong influence on the model performance. The results presented here highlight the importance of the model capability to correctly predict subgrid-scale meteorological phenomena, such as convective updrafts, downdrafts, and density currents, as a prerequisite for a realistic initiation of dust emissions into the atmosphere.

References

Ament, F., S. Crewell, and C. Simmer (2004), Impact of horizontal model resolution on cloud parameters forecasted by a non-hydrostatic mesoscale models, paper presented at the 14th International Conference on Clouds and Precipitation (ICCP), Bologna, Italy, Jun. (Available at http://www.meteo.uni-bonn.de/mitarbeiter/CSimmer/publist/documents/amentetal2004.pdf)

Barthlott, C., U. Corsmeier, C. Meißner, F. Braun, and C. Kottmeier (2006), The influence of meso-scale circulation systems on triggering convective cells over complex terrain, *Atmos. Res.*, *81*, 150–175.

Cakmur, R. V., R. L. Miller, and O. Torres (2004), Incorporating the effect of small-scale circulations upon dust emission in an atmospheric general circulation model, *J. Geophys. Res.*, *109*, D07201, doi:10.1029/2003JD004067.

Dinku, T., S. Chidzambwa, P. Ceccato, S. J. Connor, and C. F. Ropelewski (2008), Validation of high-resolution satellite rainfall products over complex terrain, *Int. J. Remote Sens.*, *29*, 4097–4110.

Doms, G., and U. Schättler (2002), *A Description of the Nonhydrostatic Regional Model LM. Part I: Dynamics and Numerics*, Deutscher

Wetterdienst, Geschäftsbereich Forschung und Entwicklung, Offenbach, Germany. (Available at http://www.cosmo-model.org/)

Doms, G., J. Förstner, E. Heise, H. J. Herzog, M. Raschendorfer, R. Schrodin, T. Reinhardt, and G. Vogel (2005), *A Description of the Nonhydrostatic Regional Model LM. Part II: Physical Parameterization*, Deutscher Wetterdienst, Geschäftsbereich Forschung und Entwicklung, Offenbach, Germany. (Available at http://www.cosmo-model.org/)

Gillette, D. A., and R. Passi (1988), Modelling dust emission caused by wind erosion, *J. Geophys. Res.*, *93*, 14,233–14,242.

Ginoux, P., M. Chin, I. Tegen, J. Prospero, B. Holben, O. Dubovik, and S.-J. Lin (2001), Sources and distributions of dust aerosols simulated with he GOCART model, *J. Geophys. Res.*, *106*, 20,255–20,273.

Heinold, B., J. Helmert, O. Hellmuth, R. Wolke, A. Ansmann, B. Marticorena, B. Laurent, and I. Tegen (2007), Regional modelling of Saharan dust events using LM MUSCAT: Model description and case studies, *J. Geophys. Res.*, *112*, D11204, doi:10.1029/2006JD007443.

Heinold, B., et al. (2009), Regional Saharan dust modelling during the SAMUM 2006 campaign, *Tellus B*, *61*(2), 307–324, doi:10.1111/j.1600-0889.2008.00387.x.

Helmert, J., B. Heinold, I. Tegen, O. Hellmuth, and M. Wendisch (2007), On the direct and semidirect effects of Saharan dust over Europe: A modeling study, *J. Geophys. Res.*, *112*, D13208, doi:10.1029/2006JD007444.

Huebener, H., K. Born, and M. Kerschgens (2007), Downscaling heavy rainfall in the subtropics—A simple approach for dynamical nesting, *Adv. Geosci.*, *10*, 9–16.

Kahn, R., et al. (2009), Desert dust aerosol air mass mapping in the 1 western Sahara, using particle properties derived from space-based multi-angle imaging, *Tellus B*, *61*(1), 239–251, doi:10.1111/j.1600-0889.2008.00398.x.

Kain, J. S. (2004), The Kain-Fritsch convective parameterization: An update, *J. Appl. Meteorol.*, *43*, 170–181.

Kain, J., and J. Fritsch (1993), Convective parameterization for mesoscale models: The Kain-Fritsch scheme. The representation of cumulus convection in numerical models, *Meteorol. Monogr.*, *24*, Am. Meteorol. Soc., 165–170.

Kandler, K., et al. (2009), Size distributions, mass concentrations, chemical and mineral composition and optical parameters of the boundary layer aerosol at Tinfou, Morocco, during SAMUM 2006, *Tellus B*, *61*(1), 32–50, doi:10.1111/j.1600-0889.2008.00385.x.

Knippertz, P., C. Deutscher, K. Kandler, T. Müller, O. Schulz, and L. Schütz (2007), Dust mobilization due to density currents in the Atlas region: Observations from the SAMUM 2006 field campaign, *J. Geophys. Res.*, *112*, D21109, doi:10.1029/2007JD008774.

Knippertz, P., et al. (2009), Dust mobilization and transport in the northern Sahara during SAMUM 2006—A meteorological overview, *Tellus B*, *61*(1), 12–31, doi:10.1111/j.1600-0889.2008.00380.x.

Kuo, H.-L. (1965), On the formation and intensification of tropical cyclones trough latent heat release by cumulus convection, *J. Atmos. Sci.*, *22*, 40–63.

Laurent, B., B. Marticorena, G. Bergametti, J. Léon, and N. Mahowald (2008), Modeling mineral dust emissions from the Sahara desert using new surface properties and soil database, *J. Geophys. Res.*, *113*, D14218, doi:10.1029/2007JD009484.

Reinhardt, T. (2005), A prognostic graupel microphysics scheme for high-resolution NWP, paper presented at 6th International SRNWP-Workshop on Nonhydrostatic Modelling, Bad Orb, Germany, Sept. 2007.

Schladitz, A., T. Müller, A. Maßling, N. Kaaden, K. Kandler, and A. Wiedensohler (2009), Measurements of insitu optical properties at Tinfou (Morocco) during the Saharan Mineral Dust Experiment SAMUM 2006, *Tellus B*, *61*(1), 64–78, doi:10.1111/j.1600-0889.2008.00397.x.

Shao, Y., M. R. Raupach, and P. A. Findlater (1993), Effect of saltation bombardment on the entrainment of dust by wind, *J. Geophys. Res.*, *98*, 12,719–12,726.

Simpson, J., C. Kummerow, W.-K. Tao, and R. F. Adler (1996), On the Tropical Rainfall Measuring Mission (TRMM), *Meteorol. Atmos. Phys.*, *60*, 19–36.

Solomon, S., D. Qin, M. Manning, M. Marquis, K. Averyt, M. M. B. Tignor, and H. L. Miller (Eds.) (2007), *Climate Change 2007: The Physical Science Basis*, 989 pp., Cambridge Univ. Press, New York.

Steppeler, J., G. Doms, U. Schättler, H. W. Bitzer, A. Gassmann, U. Damrath, and G. Gregoric (2003), Meso-gamma scale forecasts using the nonhydrostatic model LM, *Meteorol. Atmos. Phys.*, *82*, 75–96.

Tegen, I., S. P. Harrison, K. E. Kohfeld, I. C. Prentice, M. C. Coe, and M. Heimann (2002), Impact of vegetation and preferential source areas on global dust aerosols: Results from a model study, *J. Geophys. Res.*, *107*(D21), 4576, doi:10.1029/2001JD000963.

Tegen, I., B. Heinold, M. Todd, J. Helmert, R. Washington, and O. Dubovik (2006), Modelling soil dust aerosol in the Bodele depression during the BoDEx campaign, *Atmos. Chem. Phys.*, *6*, 4345–4359.

Tiedtke, M. (1989), A comprehensive mass flux scheme for cumulus parameterization in large-scale models, *Mon. Weather Rev.*, *132*, 1779–1800.

Wolke, R., O. Hellmuth, O. Knoth, W. Schröder, and E. Renner (2004), The parallel model system LM-MUSCAT for chemistry-transport simulations: Coupling scheme, parallelization and application, in *Parallel Computing: Software Technology, Algorithms, Architectures, and Applications*, edited by G. R. Joubert et al., pp. 363–370, Elsevier, New York.

Yanai, M., S. Esbensen, and J. Chu (1973), Determination of bulk properties of tropical cloud clusters from large-scale heat and moisture budgets, *J. Atmos. Sci.*, *30*, 611–627.

———————————

U. Cubasch, Institute for Meteorology, Free University Berlin, Carl-Heinrich-Becker-Weg 6-10, D-12165 Berlin, Germany. (cubasch@zedat.fu-berlin.de)

B. Heinold, O. Hellmuth, K. Schepanski, and I. Tegen, Leibniz Institute for Tropospheric Research, Permoserstraße 15, D-04318 Leipzig, Germany. (bernd.heinold@tropos.de; olaf.hellmith@tropos.de; kerstins@mail.tropos.de; itegen@tropos.de)

H. Huebener, Hessian Agency for Environment and Geology, Hessian Centre on Climate Change Affairs, Rheingaustraße 186, D-65203 Wiesbaden, Germany. (h.huebener@hlug.de)

P. Knippertz, Institute for Atmospheric Physics, Johannes Gutenberg University, Johann-Joachim-Becherweg 21, D-55099 Mainz, Germany. (knippertz@uni-mainz.de)

F. Reinfried, Ergo Institute of Environment, Lauensteiner Str. 42, D-01277 Dresden, Germany. (reinfrie@tropos.de; reinfried@ergo-dresden.de)